Journal of Physics and Chemistry of Solids 110 (2017) 386–393

Contents lists available at ScienceDirect

Journal of Physics and Chemistry of Solids

journal homepage: www.elsevier.com/locate/jpcs

Electrical resistivity of solid and liquid Cu up to 5 GPa: Decrease along the melting boundary

Innocent C. Ezenwa [a], Richard A. Secco [a,*], Wenjun Yong [a], Monica Pozzo [b], Dario Alfè [b,c]

[a] Department of Earth Sciences, University of Western Ontario, London, Ontario N6A 5B7, Canada
[b] Department of Earth Sciences and Thomas Young Centre, University College London, Gower Street, WC1E6BT, UK
[c] London Centre for Nanotechnology, University College London, 17-19 Gordon Street, WC1H, UK

A B S T R A C T

The electrical resistivity of high purity Cu has been investigated by both experiments and first principle calculations at pressures up to 5 GPa and at temperatures in the liquid phase up to 1730 K. The resistivity decreases with P and increases with T and our data are in very good agreement in relation to 1 atm data. Our melting temperature data agree with other experimental studies. We show that resistivity of Cu decreases along the P,T-dependent melting boundary in disagreement with prediction of resistivity invariance along the melting boundary. These findings are interpreted in terms of the competing effects of P and T on the electronic structure of liquid Cu. The electronic thermal conductivity is calculated from resistivity data using the Wiedemann-Franz law and is shown to increase with P in both the solid and liquid states but upon T increase, it decreases in the solid and increases in the liquid state.

1. Introduction

Electrical resistivity and thermal conductivity of metals characterize the nature of electron-phonon and electron-electron interaction as well as the phase state of a system. The effects of pressure (P) and temperature (T) on the electrical resistivity of a metal are usually antagonistic – resistivity decreases with P and increases with T. Combinations of P and T that offset each other to maintain constant resistivity can be found if the P- and T-coefficients of resistivity are known. A thermodynamically-based treatment of the effects of P and T on simple and other metals proposes that the electrical resistivity is constant on the P,T-dependent melting boundary [1,2]. If validated experimentally, this proposal would provide an elegant route to evaluate the electrical resistivity of a metal at very high P,T on its melting boundary by measuring the resistivity on the melting boundary at lower P,T. The present study provides an experimental assessment of this proposal using Cu as a test simple metal.

The theory of electrical resistivity of transition metals in the solid state is generally understood in the context of *s-d* scattering [3]. In metals, valence electrons are delocalised and are distributed over a range of energy bands. At T above 0 K, thermal vibrations of the lattice reduce the mean free path of an electron by increasing the probability of phonon-electron scattering. Although the resistivity of a metal is approximately proportional to the absolute T above the Debye T, as predicted by Bloch theory, there are deviations at very high T due to thermal expansion. The resistivity can saturate at high T in some metals when the Ioffe-Regel condition, equivalence of electron mean free path and inter-atomic spacing, is met [4,5]. With increasing P, the amplitude of atomic vibration decreases and in metals, this reduces electron scattering by phonons. This in turn causes an increase in the mean free path of the electrons and a lower resistivity.

The nearly free electron (NFE) model of Ziman's theory [6] has accounted very well for the electrical resistivity of a simple liquid metal like Cu. The transport coefficients in this theory depend on two main factors, namely, the electron ion pseudopotential matrix element, which describes electron-ion core scattering, and the dynamical structural factor of the ion system. Provided an appropriate electron-ion pseudopotential is used in the NFE model, the electrical resistivity of liquid transition metals can be well described. However for pure liquid transition metals, a different model was suggested by Mott [7], that is similar to the *s-d* transition model used in his solid state theory [3], but with different mean free paths for the *s-p* and for *d* electrons. Other theoretical studies of electron scattering in liquid transition metals [8–12] have focused on a transition-matrix term in addition to the electron ion pseudopotential in the Ziman formula [6].

For Cu with filled *3d*-band states and with an electronic configuration of $[Ar]3d^{10}4s^{1}$, the only electron-electron scattering present is *s-s* scattering, while the conduction *s* electrons of those metals with an unfilled *d*-band can undergo both *s-s* and *s-d* scattering processes. Electron mobility in the *s*-band is greater than in the *d*-band, thus, metals with

* Corresponding author.
E-mail address: secco@uwo.ca (R.A. Secco).

http://dx.doi.org/10.1016/j.jpcs.2017.06.030
Received 7 March 2017; Received in revised form 28 April 2017; Accepted 29 June 2017
Available online 1 July 2017

filled *d*-bands are generally more conductive, since s-d scattering is absent, than those with unfilled *d*-bands. The delocalised conduction electrons in a metal are subjected to a periodic electron density pattern and hence encounter scattering from it similar to that caused by the pseudopotential of the ion cores [13]. However, in the liquid state, the electron gas is best described outside the ion cores by simple plane waves that are randomly phased and isotropically propagated in a short range ordered structure [13]. In Cu, the filled *d*-band overlaps the bottom of the *s*-band and hence influences the conduction *s* electrons by shielding them from the influence of the nucleus [14,15] and simultaneously contributes to the periodic electron density of the crystal system.

The interpretation of P effects on the electronic transport of metals generally requires an understanding of the way in which P affects the Fermi surface. The notion that the Fermi surface of solid Cu may touch the Brillouin Zone (BZ) boundary was confirmed by a study of the anomalous skin effect [16]. The energy function changes near the zone boundaries and thus, the Fermi velocity is expected to be lower than its free electron value at the zone boundaries [14]. When a metal is compressed, the volume of the BZ in reciprocal space, and with it the volume enclosed by the Fermi surface, increases. A change in the dimensions of the BZ causes size and topological changes in the Fermi surface of a metal with a non-isotropic compressible crystal structure. Nonetheless, for a cubic crystal like Cu which should compress isotropically, a change in the size of the BZ ideally should cause no topological change in the Fermi surface [17]. The effect of low hydrostatic P on the Fermi surface of solid Cu has been experimentally studied [17,18] by observing the phase change in de Haas van Alphen (dHvA) oscillations in the P range of 0.0001–0.0025 GPa at 1 K and theoretically [19] using *ab initio* linear muffin-tin orbital method in the atomic sphere approximation. From the rigid-sphere model of liquid metals [20,21], the Fermi surface of many liquid metals is spherical and of volume sufficient to accommodate all the valence electrons. A study on the change of separation of the *d*-band position relative to the Fermi level (E_{Fd}) of Cu up to 1.2 GPa at room T, by observing the P-dependent shift in the reflectivity edge [22], demonstrated an increasing E_{Fd} with increasing P. Since the upper *d*-band is radially symmetric [15], the onset of separation occurs simultaneously over the entire Fermi surface. However, T-dependent investigation of the optical properties of liquid Cu at 1 atm by the polarimetric method [23] demonstrated that the *d*-band is unbroadened and unshifted relative to the Fermi level by the process of melting. This suggests that the null effect of T on E_{Fd} at the melting boundary may not compensate for the P-induced increase of E_{Fd} in Cu.

The T-dependence of electrical resistivity of solid and liquid Cu at 1 atm as reported by many different authors has been compiled by Matula [24]. The P-dependence of electrical resistivity of solid Cu has been studied by both shock wave [25–28] and static [29] P techniques. In order to investigate further the effects of P and T on the electrical resistivity of Cu, particularly in the liquid state, and to test experimentally the thermodynamics-based prediction of constant resistivity on the P-dependent melting boundary [1,2], we measured the electrical resistivity of solid and liquid Cu up to 5 GPa and 1730 K. We also performed first principles calculations based on density functional theory (DFT) and the Kubo-Greenwood (KG) approach, to compute the electrical resistivity and the thermal conductivity on liquid Cu on the melting curve at 0 and 5 GPa.

2. Experimental details

Experiments were performed in a 1000-ton cubic anvil press as described elsewhere [30]. The four-wire resistivity measurement technique and the cubic pressure cell design are illustrated in Fig. 1. Pyrophyllite was used as the P-transmitting medium and the sample pressure was determined from hydraulic oil pressure using prior unpublished calibrations similar to those previously described [30,31]. The dimensions of the Cu wire (99.99% purity, Alfa Aesar) were 0.51 mm in diameter and 1.78 mm in length. The junctions of two W5%Re-W26%Re thermocouples, which also served as 4-wire electrodes, were in direct contact with the ends of the wire sample which was contained in boron nitride (BN). Boron nitride was also used to contain the thermocouples and provided a tight seal at the metal–ceramic interface which helped in containing the liquid above the melting T. The sample length was 0.05 mm longer than the BN sample container which provided good thermocouple/electrode-sample contact. A cylindrical graphite sleeve surrounding the sample container acted as a heat source when a high alternating current was passed through it. A cylindrical zirconia (ZrO_2) sleeve and two ZrO_2 disks placed on top and bottom of the sample

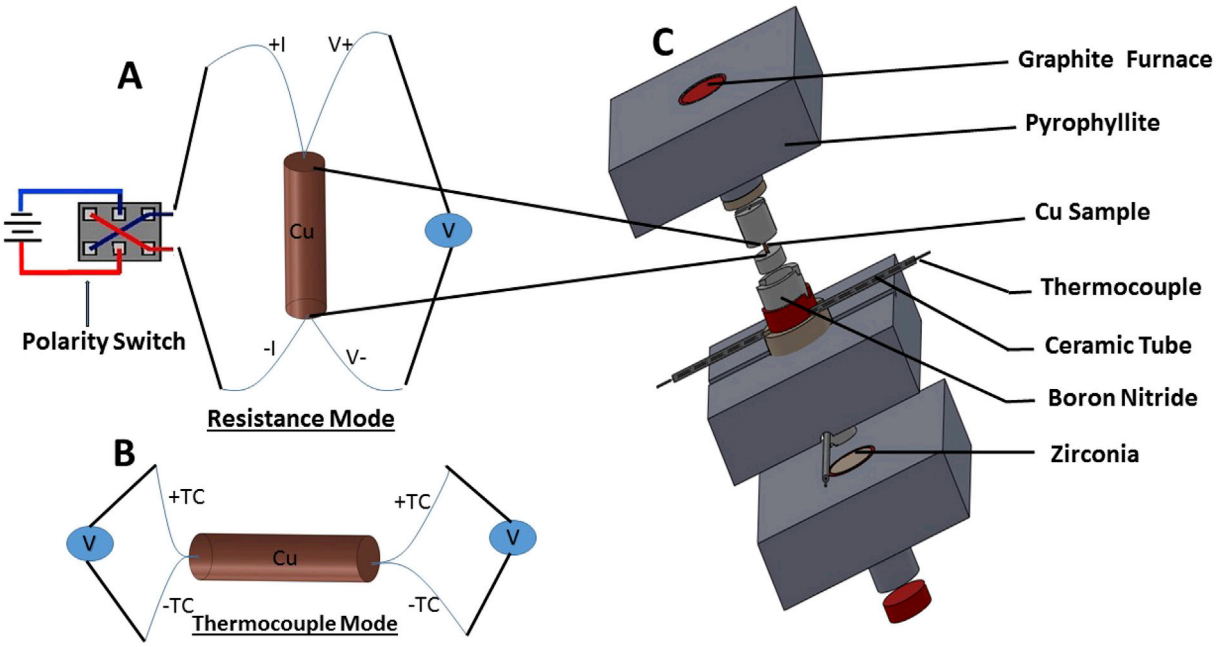

Fig. 1. Schematic drawing of two modes (resistance (A) and temperature (B)) of measurement. (A) Four–wire probe design, showing the current polarity switch and the voltmeter for measuring the voltage drop across the sample. (B) Thermocouples measuring the temperature on top and bottom of the sample. (C) SolidWorks™ design of the high-pressure cubic cell (1.25 inch edge length) with the components parts.

container provided thermal insulation. The softening of the sample and the electrodes at high T provided good sample-electrode contact thereby minimizing the effect of contact resistance. To ensure good contact was made prior to recording data, a pre-heating cycle was carried out up to T of ~1000 K at the experimental run pressure.

Ideally, two pairs of opposite faces of a cubic P-cell are needed to make a 4-wire resistivity measurement. With one pair of cube faces dedicated to the heater, and another pair needed for T measurement, a straightforward 4-wire electrode system was not possible. Our solution was to use the thermocouples as T sensors in one mode of measurement and 4-wire electrodes in another mode. A switched circuit passed a constant direct current of 0.2 A (Keysight B2961A power source) through the W5%Re leads and sample and measurement of the voltage drop was made using the W26%Re leads while the switch was in resistance mode (Fig. 1A). In T mode, the thermocouple EMF's at the top and bottom of the sample were used to measure T (Fig. 1B). In resistance mode, systematic errors in the voltage drop across the sample from the thermoelectric voltage between the sample and the electrodes were corrected by reversing the current direction with the use of a polarity switch. The mean value of the measured voltages in both current directions was computed at each T. A Keysight 34470 A data acquisition meter, operating at a frequency of 20 Hz with 1 μV resolution, was used to make measurements at 50 K intervals in the solid state and at 20 K intervals in the liquid state. The decrease in measurement interval in the liquid state was aimed at getting enough data to define a T-dependence of resistivity before the sample geometry could change caused by liquid movement. The acquired data were processed to calculate sample resistivity in the usual manner using Ohm's law, $R = \frac{V}{I}$, where R is resistance, V is voltage drop and I is current. The sample resistivity (ρ) was calculated by incorporating the recovered sample geometry into Pouillet's law $\rho = \frac{RA}{l}$, where l and A are sample length and cross-sectional area, respectively. After each run, the recovered P cell was ground along the length of the sample to expose the middle section of the sample. The length and diameter of the exposed sample were carefully measured at several locations using a Nikon SMZ2800 microscope. The chemical composition of the recovered sample and electrodes was determined by wavelength dispersive X-ray spectroscopy using a JEOL JXA-8530F field-emission electron microprobe. An accelerating voltage of 20 kV, a probe current of 50 nA, and a spot size (~100 nm) beam were used for all analyses.

3. Theoretical details

First principles simulations were performed using the VASP code [32], with the projector augmented wave (PAW) method [33,34] and the PBE [35] functional. Most calculations were performed with a Cu PAW with the $[Ar]d^{10}s^1$ valence electronic configuration, but we also tested the effect of including the 3p electrons in valence, which showed an undetectable effect on the conductivities. Single particle orbitals were expanded in plane-waves with a cutoff of 273 and 369 eV for the PAW's with the $[Ar]d^{10}s^1$ and $[Ne]p^6d^{10}s^1$ valence electronic configurations respectively. The core radii were 1.22 and 1.06 Å. Electronic levels were occupied according to Fermi-Dirac statistics, with an electronic temperature of 0.117 and 0.128 eV at the two points on the melting curve (P,T) = (0 GPa, 1350 K) and (P,T) = (5 GPa, 1490 K), respectively. An efficient extrapolation of the charge density was used to speed up the *ab initio* molecular dynamics (AIMD) simulations [36], which were performed by sampling the BZ with the Γ point only. The temperature was controlled with a Nosé thermostat [37] and the time step was set to 2 fs. To prepare the liquid systems we carried out the following procedure. First, we constructed a 3 × 3 × 3 supercell of face-centered-cubic Cu in a simple cubic setting (108 atoms). We melted the system by running an AIMD simulation for several ps at a temperature of about 5 times the melting temperature, using a volume near the expected zero pressure volume at the melting point. After melting we reduced the temperature to 1350 K, allowed the system to thermalize for 2 ps, and simulated for an additional 5 ps Liquid diffusivity was checked throughout by monitoring the mean square displacement. We then constructed an embedded-atom-model (EAM) [38] by fitting the model to the AIMD simulation, following the procedure outlined in Ref. [39]. The form of the EAM was:

$$E_{tot} = \frac{1}{2}\sum_{i\neq j}\varepsilon\left(\frac{a}{r_{ij}}\right)^n - \varepsilon C\sum_i\left[\sum_{j\neq i}\left(\frac{a}{r_{ij}}\right)^m\right]^{1/2} \quad (1)$$

where r_{ij} is the distance between two atoms at positions $\boldsymbol{r}_i$ and $\boldsymbol{r}_j$ and the sums runs for all couple of atoms for which $r_{ij} < 6$ Å. The fitted parameters were $\varepsilon = 8.839\ \ 10^{-3}$ eV, $a = 3.847$ Å, $C = 84.12$, $n = 8.294$, $m = 3.493$. We then used the EAM to prepare the liquid for larger systems, including 256, 500, 864 and 1372 atoms. Once the liquids were equilibrated at the desired temperatures we switched to AIMD, performing simulations with a typical length of 20 ps, after discarding the first ps for further equilibration. The DFT-PBE densities at (p,T) = (0,1350 K) and (p,T) = (5 GPa, 1490 K) were 7505 kg m^{-3} and 7970 kg m^{-3}. From these simulations we extracted typically $N = 80$ configurations, separated by 0.25 ps. These N configurations were then used to compute the electrical and the thermal conductivity via the Kubo-Greenwood [40,41] and the Chester-Thellung-Kubo-Greenwood [42] formula, respectively, as implemented in VASP [43]. The optical conductivities were obtained by averaging over the N configurations $\{\boldsymbol{R}_i;\ i = 1,N\}$ and over $\mathbf{k}$ points in the BZ:

$$\sigma(\omega) = \frac{1}{N}\sum_{i=1}^{N}\sum_{\mathbf{k}}\sigma_{\mathbf{k}}(\omega;\boldsymbol{R}_i)W(\mathbf{k}) \quad (2)$$

where $\sigma_{\mathbf{k}}(\omega;\boldsymbol{R}_i)$ is the optical conductivity for point $\mathbf{k}$ and configuration $\boldsymbol{R}_i$, and W($\mathbf{k}$) the weighting factor of the $\mathbf{k}$-point in the BZ. Following [44], we found it convenient to use $\mathbf{k}$-points drawn from the irreducible wedge of the BZ (IBZ) of the same system in which the atoms occupy perfect lattice positions, as convergence with respect to the number of $\mathbf{k}$-points is faster if the points are chosen in this way, provided one averages over the three Cartesian directions. The thermal conductivities were obtained using a similar procedure.

The dc conductivity σ_0 is given by the value of $\sigma(\omega)$ in the limit $\omega\rightarrow 0$. This limit needs to be taken with care, because at very small values of ω the conductivity falls unphysically to zero due to the artificial finite spacing between the Kohn-Sham eigenvalues, caused by the finite size of the simulation cell. To take this limit, our procedure is to fit the conductivity to a smooth function, without including in the fit values of $\sigma(\omega)$ that have started to fall to zero. For a simple free electron metal the natural choice would be a Drude model: $\sigma(\omega) = \sigma_0/(1+\omega^2\tau^2)$. Although Cu is not a simple metal, and a Drude model would not be appropriate to describe its optical conductivity, we found that by including in the fit a sufficiently restricted set of data in the low energy region of the spectrum the Drude model provided a convenient way to obtain the dc conductivity σ_0, and from this the resistivity $\rho_0 = 1/\sigma_0$.

4. Results and discussion

Measurements of the T-dependence of the electrical resistivity of Cu at P of 2–5 GPa and at T up to 300 K above the melting point are shown in Fig. 2. In comparison with the recommended 1 atm data by Matula [24], our high P data show very good agreement both in the solid and liquid states and they demonstrate the expected T- and P-effects on resistivity. The abrupt increase in resistivity marks the solid-liquid transition in Cu. The melting T at a fixed P was determined by taking the average of the T measured at the start and completion of melting. Our melting T determined at 2 GPa in this way agrees with previous experimental studies carried out in large volume presses and in diamond anvil cells [45–48] as shown in Fig. 3. However our data show a maximum deviation of ~5.2% at 5 GPa with the average of the other data sets. The melting point differences between our results and the other experimental studies are probably caused by the high rates of heating, polarity switching rate and

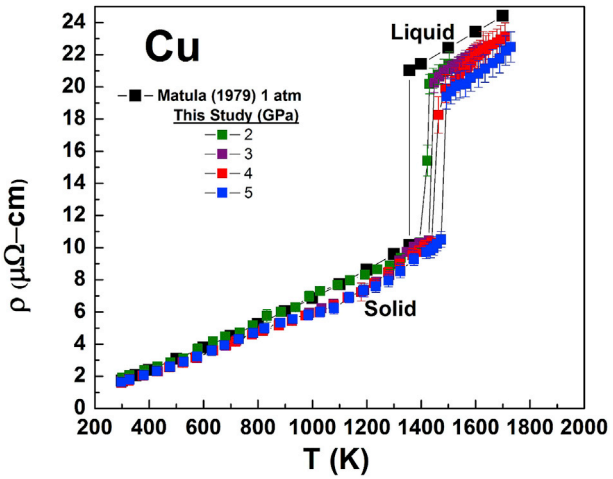

Fig. 2. Temperature dependence of electrical resistivity of Cu at fixed pressures compared with 1 atm data from several studies as recommended by Matula [24].

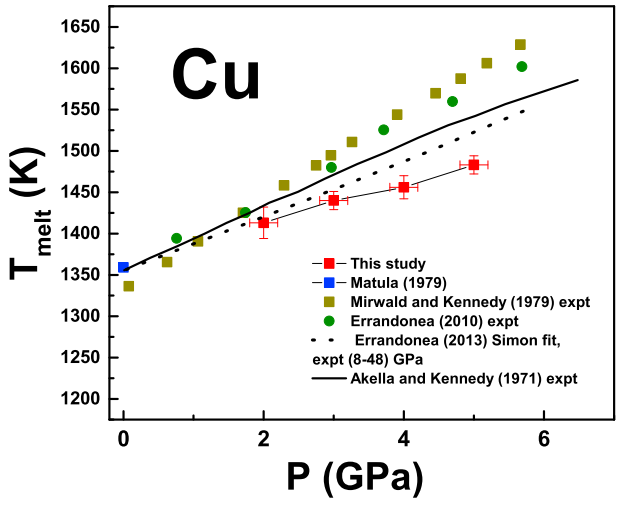

Fig. 3. Melting curve of Cu up to 5 GPa, determined by the jump in resistivity in this study, compared with previous studies.

the positions of the thermocouples which are ~0.7 mm away from the hottest (i.e. central) part of the sample in our experiments.

Though measurements were made with one design of pressure cell and strict adherence to one experimental procedure, there were typically slight but significant differences in the geometry between successive sample assemblies after high P and T exposure. These require correction by careful inspection of the recovered sample and measurement of its geometry under microscope as shown in Fig. 4A. These geometry values were used as input into the calculation of the resistivity. It is evident from microprobe analyses of the recovered sample, an example of which is shown Fig. 4B, there was no contamination of the sample either by the electrode/thermocouple or container material. These microprobe results are consistent with the phase diagram of the Cu-W binary system [49] and the absence of any interaction of liquid Cu and Re [50].

As expected, the resistivity of Cu decreases with increasing P in the solid state as shown by the isothermal resistivity behavior at 1350 K in

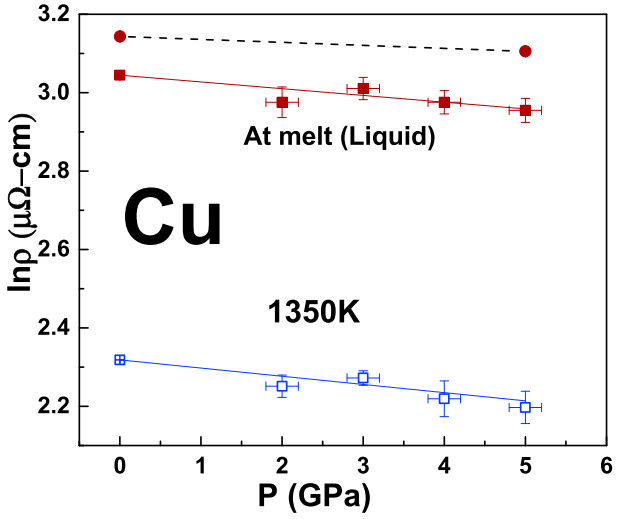

Fig. 5. P-dependence of electrical resistivity of Cu in the solid state along the 1350 K isotherm (open squares) and in the liquid state along the melting boundary (filled squares are experimental; circles are calculation - errors within symbol size). The calculated slopes for the pressure coefficient of resistivity of the experimental data are $(d\ln \rho/dP)_{1350K} = -0.021 \pm 0.003$ GPa^{-1} and $(d\ln \rho/dP)_{\text{melt boundary}} = -0.017 \pm 0.003$ GPa^{-1}. Experimental data at 1 atm are from Matula [24].

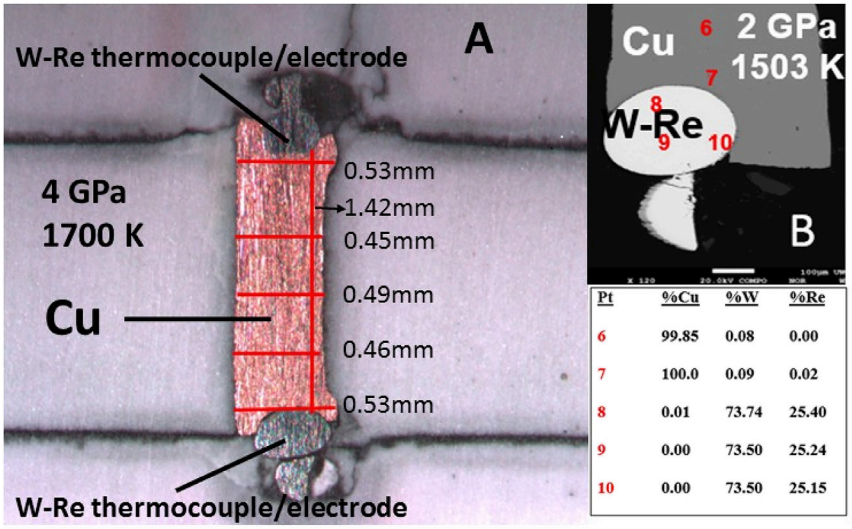

Pt	%Cu	%W	%Re
6	99.85	0.08	0.00
7	100.0	0.09	0.02
8	0.01	73.74	25.40
9	0.00	73.50	25.24
10	0.00	73.50	25.15

Fig. 4. (A) Post-mortem view of a sectioned pressure cell recovered from 4 GPa to 1700 K. Thermocouple/electrodes were W5%Re and W26%Re. Measurements of the length and width at several locations of the ground Cu sample are labelled. (B) Back scattered electron image of a sample recovered from 2 GPa, 1503 K along with tabulated electron microprobe results of probe points 6–10. The white scale bar is 100 μm.

Fig. 5. The electronic structure of Cu has been very well investigated both experimentally and theoretically [51–58]. Studies have shown that the interaction between the high-lying *3d*-band and the *s* conduction band leads to appreciable distortion of the Fermi surface of Cu from a perfect sphere, giving rise to neck features [15,59]. Experiments probing the dHvA oscillations of the magnetic susceptibility and theoretical studies on the effect of P on the Fermi surface of Cu have shown that the neck section increases relative to the bellies [17–19]. The increased distortion of the Fermi surface with P promotes zone boundary scattering which diminishes the mean free path of the electrons near the Fermi energy and enhances the electrical resistivity. However on any given isotherm, the effect of P-induced increase of E_{Fd} [22], which decreases the scattering caused by the reduced influence of the periodic electron density on the conduction *s* electrons as well as the P-induced reduction of the phonon amplitude, causes a net decrease in resistivity in the solid state.

The resistivity at the solid-liquid phase transition doubles in value as shown in the resistivity ratio plotted versus P in Fig. 6. Other metals similar to Cu in crystal and electronic structure, such as Ag and Au, show similar doubling of the resistivity on melting at 1 atm [24]. From the NFE model [6], the relative change in electrical resistivity during melting is caused by the change in the radial distribution function of the ions which results in larger ion scattering cross-sections. T-variation of resistivity in the liquid state follows from the T-dependent Fourier transform of the radial distribution function, or structure factor, of the ions in the liquid state. The spherical nature of the Fermi surface of most liquid metals [20,21] demonstrates that thermal expansion could very well compensate for the distortion effects of P on the Fermi surface of Cu on melting. If these effects were cancelling, they would cause the resistivity of Cu at the melting boundary to be constant. However, the effect of P-induced increase of E_{Fd} and the P-induced decrease of phonon amplitudes appear to dominate over effects of T as shown in the decreasing behavior of resistivity on the melting boundary in Fig. 5.

The T-coefficient of resistivity $(d\ ln\ \rho/d\ T)_P$ in the liquid state and at three temperature ranges in the solid state obtained in this study are plotted versus P in Fig. 7 and are compared with 1 atm studies. Our values are in general agreement with 1 atm values. However, there does not appear to be a P-dependent trend in any of the temperature data sets. There is no indication in the T-coefficient of resistivity behavior that would suggest a P-induced change in structure of Cu in either the solid or liquid state, in agreement with the phase diagram of Cu reported up to 6 GPa [60].

As shown in Fig. 5, the P-coefficient of resistivity on the melting boundary, $\left(\frac{\partial \ln\rho}{\partial P}\right)_{melt\ \ boundary}$ is -0.017 ± 0.003 GPa^{-1}, and the P-coefficient of resistivity along the 1350 K isotherm, $\left(\frac{\partial \ln\rho}{\partial P}\right)_{1350K}$, is -0.021 ± 0.003 GPa^{-1}. We compare our value of $\left(\frac{\partial \ln\rho}{\partial P}\right)_{1350K}$, with the value calculated using the relationship derived by Stacey and Anderson [1]:

$$\left(\frac{\partial \ln\rho}{\partial P}\right)_{1350K} = \frac{-2\ (\gamma - 1/3)}{K_T} \tag{3}$$

where γ is the Grüneisen parameter and K_T is the isothermal bulk modulus. We estimate γ to be 1.5 for solid Cu at 1350 K from the 1.96 room T measurement by Chatterjee [61] and applying T-dependence of γ by Singh [62]. With a K_T value of 134 GPa at 300 K, we extrapolate K_T to 1350 K from the T-dependence of K_T measured up to 800 K by Chang and Himmel [63], to be 93.7 GPa and calculate a value of -0.025 GPa^{-1} for $(\partial\ ln\ \rho/\partial\ P)_{1350K}$ from Eqn (3). The prediction of $(\partial\ ln\ \rho/\partial\ P)_{1350K}$ by Eqn (3) compares well with our measured experimental value. However, the value of $(\partial\ ln\ \rho/\partial\ P)_{melting\ \ boundry}$ is not equal to zero which does not support the conclusion that the electrical resistivity of an electronically simple metal such as Cu is constant on the P,T-dependent melting boundary [1,2]. Our experimental findings suggest that although electron scattering increases with both T at the melting point and with structural disorder that accompanies melting, the integrated effects of increasing P on electron scattering on melting results in an overall decrease in electrical resistivity along the melting boundary. This is clearly shown in Fig. 6 where the ratio of the liquid to solid resistivity values at the melting point is plotted versus P. With nearly constant solid resistivity just below the melting point (10.1–10.5 $\times$ 10^{-6} Ωcm) as demonstrated in Fig. 2, the decreasing resistivity in the liquid at the melting point with increasing P causes an overall decrease in the resistivity ratio.

In Fig. 8 we show the theoretical DFT-KG resistivities computed on the melting curve at ambient pressure and at a pressure of 5 GPa, as function of the size of the simulation cell. Convergence to better than ~3% is obtained with simulation cells including 500 atoms or more, and there is little difference between calculations performed with either 4 or 10 **k**-points. Statistical error bars were obtained from the spread of the values of the resistivities for each of the *N* configurations included in the calculations. The converged values are also reported in Fig. 5, which shows agreement with the experimental values to within 16%, and confirm the decrease of resistivities as function of pressure on the melting

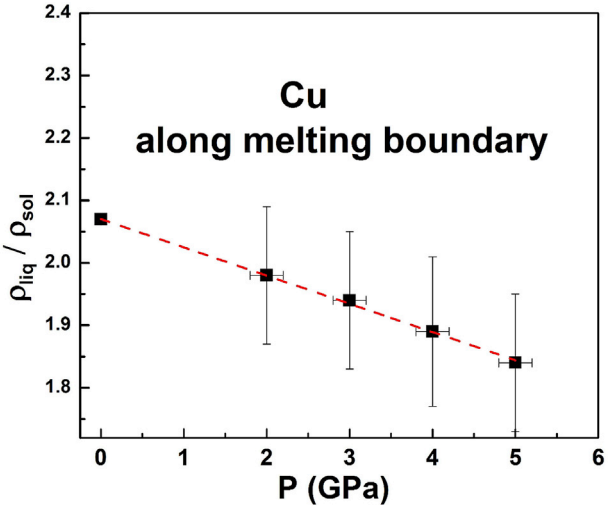

Fig. 6. P-dependence of the resistivity ratio of liquid to solid at the melting point. Least squares fit ($r^2 = 0.998$) yields $\rho_{liq}/\rho_{sol} = 2.072–0.0457(0.0006)$ P GPa^{-1}.

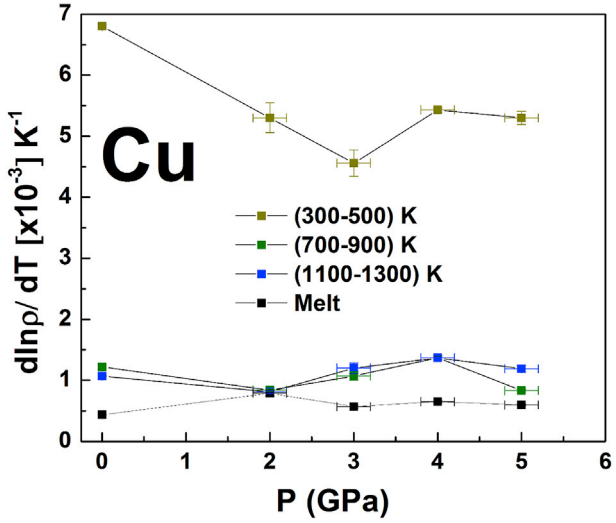

Fig. 7. The T coefficient ($d\ln\rho/dT$) of electrical resistivity plotted for liquid Cu and three temperature ranges in the solid state for P range of 2–5 GPa. Comparison is made with $dln\rho/dT$ derived from the1atm data of many studies as compiled by Matula [24]. Error bars are provided or are within the symbol size.

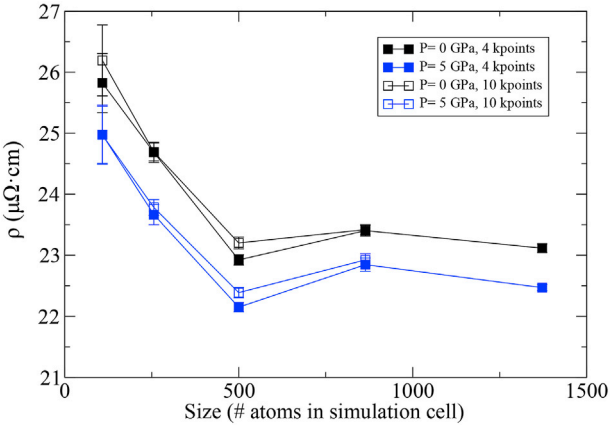

Fig. 8. Resistivities of liquid Cu at (p,T)=(0, 1350 K) (black) and (p,T)=(5 GPa, 1490 K) (blue) calculated using DFT-KG. Calculations are reported as function of the number of atoms in the simulation cell, and for two different sets of **k**-points used to sample the Brillouin Zone. (For interpretation of the references to colour in this figure legend, the reader is referred to the web version of this article.)

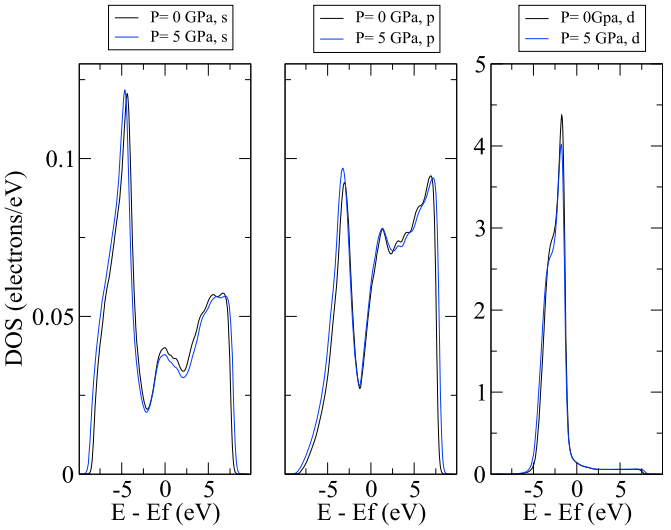

Fig. 9. DFT projected density of states of liquid Cu at (P,T)=(0,1350 K) (black) and (P,T)=(5 GPa, 1490 K) (blue). (For interpretation of the references to colour in this figure legend, the reader is referred to the web version of this article.)

curve. In Fig. 9 we show the projected density of states (pDOS) of the liquid at the two pressures. These are calculated by projecting the Kohn-Sham wavefunction onto spherical harmonics of degree 0, 1 and 2, inside spheres centered on the atoms and with a radius of 1.31 A. The pDOS are obtained by averaging over all the atoms in the simulation cell, and also averaging over several independent configurations representative of the liquids. The pDOS at 0 and 5 GPa are very similar, but it is worthwhile to point out two interesting features: i) the centre of mass of the *d* component of the pDOS is shifted towards lower energy, so that E_{Fd} is increased. As discussed above, this effect contributes to enhance the screening effect of the *d* electrons, increasing the mobility of the *s* and *p* electrons; ii) the ratios between the weights of the *s* and *p* components to that of the *d* component of the pDOS are also enhanced by pressure, which results in an increase of the number of the more mobile *s* and *p* electrons compared to *d* electrons. Both these effects contribute to reduce the overall resistivity of the liquid at increased pressure.

There exist only few data on the direct measurement of thermal conductivity of Cu at high T and/or P [64–68]. This is primarily because of the challenges in maintaining a small T gradient at high T. At high T in the solid state and in the liquid state, there is an additional challenge of chemical contamination. At high P conditions, the challenges rise sharply. Hence, indirect measurement and/or determination of the thermal conductivity at these conditions are desirable. The phonon contribution, k_P, to the total thermal conductivity, k_{total}, in a metal is generally negligible compared to the dominant contribution by the electrons, k_e [69]. Fortunately, the electrical resistivity is approximately related to the electronic thermal conductivity through the Wiedemann - Franz law [70], $k_e = \frac{LT}{\rho}$ where L is the Lorenz number. Above the Debye T, the Lorenz number for solid Cu approaches the Sommerfeld value of $2.445 \times 10^{-8}\ V^2/K^2$ [71,72].

The electronic thermal conductivity, k_e, of Cu was calculated from our experimental electrical resistivity data using the Wiedemann-Franz law and using the Sommerfeld value of $L\left(2.445 \times 10^{-8}\frac{V^2}{K^2}\right)$. The T-dependence of k_e at four P values is shown in Fig. 10. We compare our results of k_e with those calculated in the same way using the 1 atm electrical resistivity data of Matula [24]. As expected, k_e decreases with increasing T in the solid state. On melting, k_e decreases to approximately half of its solid state value and in the liquid state k_e increases slightly with T. With increasing P, k_e increases both in the solid and liquid state. Also plotted on Fig. 10 for comparison are the recommended values of total thermal conductivity, k_{total}, at 1 atm from experimental studies as collected in Ho et al. [67]. These values are recommended from a number of experimental studies and are expected to be accurate to within ±4% in the solid

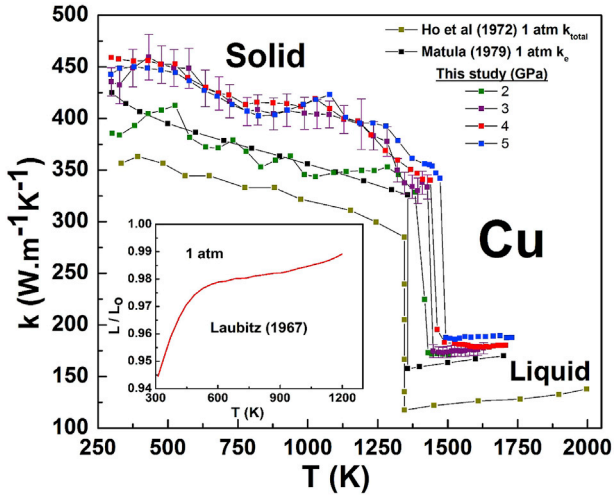

Fig. 10. Temperature dependence of the thermal conductivity at various pressures. The electronic component (k_e) was calculated from our electrical resistivity data using the Wiedemann-Franz law and the Sommerfeld value $\left(2.445 \times 10^{-8}\frac{V^2}{K^2}\right)$ of the Lorenz number. Representative error bars are shown for the 3 GPa dataset. Comparison is made with the electronic thermal conductivity based on Matula [24] resistivity data at 1 atm and with the total thermal conductivity (k_{total}) from experimental measurements reported in Ho et al. [67]. The inset figure shows the T-dependence of the measured Lorenz number for Cu [Laubitz [66]].

state and ±15% in the liquid state [67]. The 1 atm experimental values of k_{total} are lower than the values of k_e calculated from electrical resistivity using the Wiedemann-Franz Law. This is unexpected since k_{total} is the sum of k_e and k_p. This suggests that the Sommerfeld value of the Lorenz number may not be valid for Cu at these T as shown for other metals [73]. The insert plot in Fig. 10 indeed shows that the experimentally derived Lorenz number [66] varies with T for Cu and remains below the Sommerfeld value at T up to 1200 K. The use of this Lorenz function would lower k_e calculated from electrical resistivity but would not completely reconcile the difference between the values of k_{total} [67] and k_e from Ref. [24] and this study. On the other hand, the experimental study by Starr [65] indicates that the Wiedemann-Franz ratio for Cu up to a P range of 1.1 GPa has a very small positive P-coefficient from the contribution of k_p.

The calculated electronic contribution to the thermal conductivities

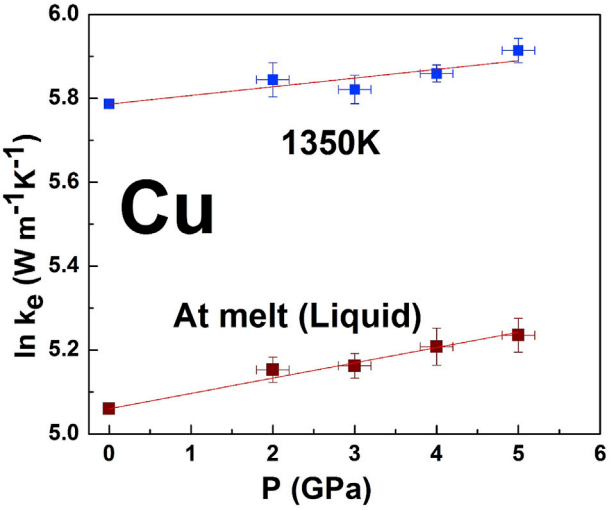

Fig. 11. P-dependence of thermal conductivity of Cu at 1350 K and along the melting boundary. The calculated slopes for the pressure coefficient of electronic thermal conductivity k_e, of the fitted lines are $(d\ln k_e/dP)_{1350K} = (0.021 \pm 0.003)$ GPa^{-1} and $(d\ln k_e/dP)_{\text{melt boundary}} = (0.038 \pm 0.002)$ GPa^{-1}.

are 137.5 (4) and 152.5 (5) W m^{-1} K^{-1}, from which we obtain values for the Lorenz number of 2.367(14) $\times$ 10^{-8} and 2.347(18) x 10^{-8} at 0 GPa, 1350 K and 5 GPa, 1490 K, respectively. Both sets of values are in good agreement with values derived from experimental measurements as shown in Fig. 10. The calculated Lorenz number values are somewhat lower than the Sommerfeld value of 2.443 $\times$ 10^{-8} W m^{-1} K^{-1}, and are constant on the melting curve within statistical error.

As shown in Fig. 11, the P-dependence of k_e is plotted at, 1350 K and at melt. We calculate a P-coefficient of k_e, $\left(\frac{\partial \ln k_e}{\partial P}\right)_{melt}$ of 0.038±0.002 GPa^{-1} and $\left(\frac{\partial \ln k_e}{\partial P}\right)_{1350K}$ of 0.021±0.003 GPa^{-1} from our data. We compare this value with the same parameter calculated using the relationship derived by Bohlin [74] given in Eqn (4), which is similar to Eqn (1) for electrical resistivity:

$$\left(\frac{\partial \ln k_e}{\partial P}\right)_T = \frac{(2\gamma - 1/3)}{K_T} \tag{4}$$

We calculate a value of 0.038 GPa^{-1} for $(\partial \ln k_e/\partial P)_{1350K}$ from Eqn (4). The prediction of $(\partial \ln k_e/\partial P)_{1350K}$ by Eqn (4) is reasonably close to our measured value. Our experimental findings suggest that although electron mobility decreases with both T on the melting boundary and with structural disorder that accompanies melting, the integrated effects of increasing P on k_e on melting results in an overall increase in k_e.

5. Conclusions

The T-dependence of electrical resistivity of Cu in both solid and liquid states has been investigated up to P of 5 GPa. Our results show that the electrical resistivity at the melting T decreases as a function of P in contrast to prediction. These findings are interpreted in terms of the antagonistic effects of P and T on the electronic structure of liquid Cu as demonstrated in previous studies and reviewed in the introduction section of this manuscript The electronic thermal conductivity was calculated using the Wiedemann-Franz law with the Sommerfeld value of the Lorenz number. The electronic component of thermal conductivity increases with P both in the solid and liquid states and at fixed P, it decreases as a function of T in the solid state, but increases with T in the liquid state. Comparison of the calculated electronic thermal conductivity and experimentally measured total thermal conductivity at 1 atm indicates that phonon conductivity is very low in Cu. Within experimental error, our melting T at P values up to 5 GPa are in agreement with previous experimental studies.

Acknowledgements

We thank Jon Jacobs for help with experiments and RAS acknowledges NSERC for a Discovery Grant number 105604-2013. The DFT calculations were performed on the UK national service ARCHER, the UK's national high-performance computing service, which is funded by the Office of Science and Technology through EPSRC's High End Computing Programme. This research also used resources of the Oak Ridge Leadership Computing Facility located in the Oak Ridge National Laboratory, which is supported by the Office of Science of the Department of Energy under Contract No. DE-AC05-00OR22725. The work of M. P. was supported by NERC Grant number NE/M000990/1.

References

[1] F.D. Stacey, O.L. Anderson, Electrical and thermal conductivities of Fe–Ni–Si alloy under core conditions, Phys. Earth Planet. Interiors 124 (3) (2001) 153–162.
[2] F.D. Stacey, D.E. Loper, A revised estimate of the conductivity of iron alloy at high pressure and implications for the core energy balance, Phys. Earth Planet. Interiors 161 (1) (2007) 13–18.
[3] N.F. Mott, The electrical conductivity of transition metals, Proc. R. Soc. Lond. A Math. Phys. Eng. Sci. 153 (880) (1936) 699–717.
[4] A.F. Ioffe, A.R. Regel, Non-crystalline, amorphous and liquid electronic semiconductors, Prog. Semicond. 4 (1960) 237–291.
[5] O. Gunnarsson, M. Calandra, J.E. Han, Colloquium: saturation of electrical resistivity, Rev. Mod. Phys. 75 (2003) 1085–1099.
[6] J.M. Ziman, A theory of the electrical properties of liquid metals. I: the monovalent metals, Philos. Mag. 6 (68) (1961) 1013–1034.
[7] N.F. Mott, The electrical resistivity of liquid transition metals, Philos. Mag. 26 (6) (1972) 1249–1261.
[8] R. Evans, D.A. Greenwood, P. Lloyd, Calculations of the transport properties of liquid transition metals, Phys. Lett. A 35 (2) (1971) 57–58.
[9] O. Dreirach, R. Evans, H.J. Guntherodt, H.U. Kunzi, A simple muffin tin model for the electrical resistivity of liquid noble and transition metals and their alloys, J. Phys. F Metal Phys. 2 (4) (1972) 709–725.
[10] K. Hirata, Y. Waseda, A. Jain, R. Srivastava, Resistivity of liquid transition metals and their alloys using the t matrix, J. Phys. F Metal Phys. 7 (3) (1977) 419–425.
[11] J.S. Ononiwu, Calculation of electrical resistivity of liquid transition metals, Phys. Status Solidi (b) 177 (2) (1993) 413–423.
[12] V.T. Shvets, S. Savenko, S. Datsko, Perturbation theory for electrical resistivity of liquid transition metals, J. Phys. Condens. Matter Phys. 5 (3) (2002) 511–532.
[13] C.C. Bradley, T.E. Faber, E.G. Wilson, J.M. Ziman, A theory of the electrical properties of liquid metals II. Polyvalent metals, Philos. Mag. 7 (77) (1962) 865–887.
[14] J.M. Ziman, Electrons and Phonons: the Theory of Transport Phenomena in Solids, Oxford Univ. Press, 1960, pp. 112–113.
[15] B. Segall, Fermi surface and energy bands of copper, Phys. Rev. 125 (1) (1962) 109–122.
[16] A.B. Pippard, An experimental determination of the fermi surface in copper, Philos. Trans. R. Soc. Lond. A Math. Phys. Eng. Sci. 250 (979) (1957) 325–357.
[17] I.M. Templeton, The effect of hydrostatic pressure on the fermi surfaces of copper, silver, and gold. II. High precision studies, Can. J. Phys. 52 (17) (1974) 1628–1634.
[18] W.J. O'Sullivan, J.E. Schirber, Experimental determination of the effect of hydrostatic pressure on the Fermi surface of copper, Phys. Rev. 170 (3) (1968) 667–669.
[19] R. Ahuja, A.K. Solanki, S. Auluck, Effect of pressure on the Fermi surface of noble metals, Phys. Rev. B 39 (14) (1989) 9806–9808.
[20] N.W. Ashcroft, J. Lekner, Structure and resistivity of liquid metals, Phys. Rev. 145 (1) (1966) 83–90.
[21] T.E. Faber, Introduction to the Theory of Liquid Metals, Cambridge University Press, 2010.
[22] R. Zallen, The effect of pressure on optical properties of the noble metals, in: Optical Properties and Electronic Structure of Metals and Alloys: Proceedings of the International Colloquium, 1966, p. 164.
[23] J.C. Miller, Optical properties of liquid metals at high temperatures, Philos. Mag. 20 (168) (1969) 1115–1132.
[24] R.A. Matula, Electrical resistivity of copper, gold, palladium, and silver, J. Phys. Chem. Ref. Data 8 (4) (1979) 1147–1298.
[25] R.N. Keeler, Electrical conductivity of condensed media at high pressures, in: P. Caldirola, H. Knoepfel (Eds.), Physics of High Energy Density, Academic Press, New York, 1971.
[26] D.D. Bloomquist, S.A. Sheffield, Shock-Compression temperature rise in polymethyl methacrylate determined from resistivity of embedded copper foils, Appl. Phys. Lett. 38 (3) (1981) 185–187.
[27] M.A. Gulevich, Measurement of electrical conductivity of copper under impulsive loading, Combust. Explos. Shock Waves 47 (6) (2011) 715–720.
[28] S.D. Gilev, V.S. Prokop'ev, Electrical resistance of copper under shock compression: experimental data, Combust. Explos. Shock Waves 52 (1) (2016) 107–116.

[29] P.W. Bridgman, The resistance of 72 elements, alloys and compounds to 100,000 Kg/Cm^2, Proc. Am. Acad. Arts Sci. 81 (No. 4) (1952, March) 165–251.
[30] R.A. Secco, High p, T physical property studies of Earth's interior: thermoelectric power of solid and liquid Fe up to 6.4GPa, Can. J. Phys. 73 (5–6) (1995) 287–294.
[31] R.A. Secco, H.H. Schloessin, On-line p, T calibration based on well-known phase transitions, J. Appl. Phys. 60 (5) (1986) 1625–1633.
[32] G. Kresse, J. Furthmüller, Efficient iterative schemes for *ab initio* total energy calculations using a plane wave basis set, Phys. Rev. B 54 (1996) 11169–11186.
[33] P.E. Blöchl, Projector augmented wave method, Phys. Rev. B 50 (1994) 17953–17979.
[34] G. Kresse, D. Joubert, From ultrasoft presudopotentials to the projector-augmented wave method, Phys. Rev. B 59 (1999) 1758–1775.
[35] J.P. Perdew, K. Burke, M. Ernzerhof, Generalized gradient approximation made simple, Phys. Rev. Lett. 77 (1996) 3865–3868.
[36] D. Alfè, Ab initio molecular dynamics, a simple algorithm for charge extrapolation, Comput. Phys. Commun. 118 (1999) 31–33.
[37] S. Nosé, A unified formulation of the constant temperature molecular-dynamics methods, J. Chem. Phys. 81 (1984) 511–519.
[38] A.P. Sutton, J. Chen, Long-range finnis-sinclair potentials, Philos. Mag. Lett. 61 (1990) 139–146.
[39] M. Pozzo, D. Alfè, Melting curve of face-centered-cubic nickel from first principles calculations, Phys. Rev. B 88 (2013) 024111.
[40] R. Kubo, Statistical-mechanical theory of irreversible processes. I. General theory and simple applications to magnetic and conduction problems, J. Phys. Soc. Jpn. 12 (1957) 570–586.
[41] D.A. Greenwood, The Boltzmann equation in the theory of electrical conduction in metals, Proc. Phys. Soc. 71 (1958) 585–596.
[42] G.V. Chester, A. Thellung, The law of Wiedemann and Franz, Proc. Phys. Soc. 77 (1961) 1005–1013.
[43] M.P. Desjarlais, J.D. Kress, L.A. Collins, Electrical conductivity for warm, dense aluminum plasmas and liquids, Phys. Rev. E 66 (2002), 025401(R).
[44] M. Pozzo, M.P. Desjarlais, D. Alfè, Electrical and thermal conductivity of liquid sodium from first-principles calculations, Phys. Rev. B 84 (2011) 054203.
[45] P.W. Mirwald, G.C. Kennedy, The melting curve of gold, silver, and copper to 60-Kbar pressure: a reinvestigation, J. Geophys. Res. Solid Earth 84 (B12) (1979) 6750–6756.
[46] D. Errandonea, The melting curve of ten metals up to 12GPa and 1600 K, J. Appl. Phys. 108 (3) (2010) 033517.
[47] D. Errandonea, High-pressure melting curves of the transition metals Cu, Ni, Pd, and Pt, Phys. Rev. B 87 (5) (2013) 054108.
[48] J. Akella, G.C. Kennedy, Melting of gold, silver and copper – proposal for a new high pressure calibration scale, J. Geophys. Res. 76 (20) (1971) 4969–4977.
[49] P.R. Subramanian, D.E. Laughlin, Cu-w (Copper-tungsten). Phase Diagrams of Binary Tungsten Alloys, 1991, pp. 76–79.
[50] J.R. Davis, ASM Specialty Handbook: Heat-resistant Materials, ASM International, 1997, p. 380.
[51] G. Baym, Direct calculation of electronic properties of metals from neutron scattering data, Phys. Rev. 135 (6A) (1964) A1691–A1692.
[52] E.I. Zornberg, F.M. Mueller, Fermi surface of copper, Phys. Rev. 151 (2) (1966) 557.
[53] P.E. Mijnarends, Determination of the Fermi surface of copper by positron annihilation, Phys. Rev. 178 (2) (1969) 622–629.
[54] J.R. Chelikowsky, M.Y. Chou, Electronic and structural properties of elemental copper: a pseudopotential–local-orbital calculation, Phys. Rev. B 38 (12) (1988) 7966–7971.
[55] Y. Zhou, W. Lai, J. Wang, Calculated electronic structure of metastable phases of Cu, Phys. Rev. B 49 (7) (1994) 4463–4466.
[56] A. Yamasaki, T. Fujiwara, Electronic structure of transition metals Fe, Ni and Cu in the GW approximation, J. Phys. Soc. Jpn. 72 (3) (2003) 607–610.
[57] M. Vos, A.S. Kheifets, C. Bowles, C. Chen, E. Weigold, F. Aryasetiawan, Electronic structure of copper studied by electron momentum spectroscopy, Phys. Rev. B 70 (20) (2004) 205111.
[58] P.B. Thakor, Y.A. Sonvane, A.R. Jani, Electronic transport properties of some transition liquid metals, Phys. Chem. Liq. 47 (6) (2009) 653–662.
[59] W.E. Spicer, C.N. Berglund, d-band of copper, Phys. Rev. Lett. 12 (1) (1964) 9.
[60] E.Y. Tonkov, E.G. Ponyatovsky, Phase transformations of elements under high pressure (Vol. 4 of Advances in Metallic Alloys; series eds. J.N. Fridlyander and D. G, Eskin), CRC press, Washington D.C., 2005, pp. 275–279.
[61] B. Chatterjee, On the relation of the Grüneisen parameter to the thermal stability of metals, Metall. Trans. A 12 (8) (1981) 1531–1534.
[62] R.N. Singh, S. Arafin, A.K. George, Temperature-dependent thermo-elastic properties of s-, p-and d-block liquid metals, Phys. B Condens. Matter 387 (1) (2007) 344–351.
[63] Y.A. Chang, L. Himmel, Temperature dependence of the elastic constants of Cu, Ag, and Au above room temperature, J. Appl. Phys. 37 (9) (1966) 3567–3572.
[64] P.W. Bridgman, The effect of pressure on the thermal conductivity of metals. In, Proc. Am. Acad. Arts Sci. 57 (5) (1922) 77–127.
[65] C. Starr, The pressure coefficient of thermal conductivity of metals, Phys. Rev. 54 (3) (1938) 210–216.
[66] M.J. Laubitz, Transport properties of pure metals at high temperatures: I. Copper, Can. J. Phys. 45 (11) (1967) 3677–3696.
[67] C.Y. Ho, R.W. Powell, P.E. Liley, Thermal conductivity of the elements, J. Phys. Chem. Ref. Data 1 (2) (1972) 279–421.
[68] B. Sundqvist, G. Bäckström, Thermal conductivity of copper under high pressure, High. Temp.-High Press. 9 (1) (1977) 41–48.
[69] P.G. Klemens, R.K. Williams, Thermal conductivity of metals and alloys, Int. Met. Rev. 31 (1) (1986) 197–215.
[70] R. Franz, G. Wiedemann, Ueber die wärme-leitungsfähigkeit der metalle, Ann. Phys. 165 (8) (1853) 497–531.
[71] J.P. Moore, D.L. McElroy, R.S. Graves, Thermal conductivity and electrical resistivity of high-purity copper from 78 to 400° K, Can. J. Phys. 45 (12) (1967) 3849–3865.
[72] B. Giordanengo, N. Benazzi, J. Vinckel, J.G. Gasser, L. Roubi, Thermal conductivity of liquid metals and metallic alloys, J. Non-Cryst. Solids 250–252 (1999) 377–383.
[73] N. de Koker, G. Steinle-Neumann, V. Vlček, Electrical resistivity and thermal conductivity of liquid Fe alloys at high P and T, and heat flux in Earth's core, Proc. Natl. Acad. Sci. 109 (11) (2012) 4070–4073.
[74] L. Bohlin, Thermal conduction of metals at high pressure, Solid State Commun. 19 (4) (1976) 389–390.